Thermoelectric properties of partially filled skutterudites RxCo4Sb12 (R = Ce and Nd) synthesized under high pressures

Thermoelectric properties of partially filled skutterudites $R_xCo_4Sb_{12}$ (R = Ce and Nd) synthesized under high pressures

Yuttana Mona[1], Jun-ichi Hayashi[1], Yukihiro Kawamura[1], Kunihiro Kihou[2], Hirotaka Nishiate[2], Chul-Ho Lee[2], and Chihiro Sekine[1*]

[1]*Muroran Institute of Technology, Muroran, Hokkaido 050-8585, Japan*

[2]*National Institute of Advanced Industrial Science and Technology (AIST) Tsukuba, Ibaraki 305-8568, Japan*

[*]E-mail: sekine@mmm.muroran-it.ac.jp

We report the thermoelectric properties of the partially Ce or Nd filled skutterudite compounds $Ce_xCo_4Sb_{12}$ and $Nd_xCo_4Sb_{12}$ prepared under high pressures and temperatures. The samples were characterized by X-ray diffraction. The actual filling ratio x of Ce or Nd was estimated by scanning electron microscopy (SEM) with energy-dispersive X-ray spectrometry (EDX). SEM-EDX results indicate that the maximum x values of Ce and Nd can be increased to 0.37 and 0.33, respectively. These values have been considered the highest for any $Ce_xCo_4Sb_{12}$ and $Nd_xCo_4Sb_{12}$ reported thus far. The electrical resistivity, thermal conductivity, and Seebeck coefficient measurements of the compounds were performed from 5 to 760 K. Furthermore, the Hall coefficient and specific heat of the compounds were also measured below 300 K. The Seebeck and Hall coefficients of both Ce- and Nd-filled samples exhibited the n-type conductor behavior. The maximum dimensionless figure-of-merit (ZT) values of $Ce_xCo_4Sb_{12}$ and $Nd_xCo_4Sb_{12}$ were determined to be 0.26 and 0.48 at 700 K, respectively.

1. Introduction

Thermoelectric (TE) materials have been utilized for power generation devices by the direct conversion of waste heat into electrical power. They have many potential applications in environmentally friendly power generation systems with advantages such as nonpolluting, long-term stability, and availability in a wide temperature range.[1–3)] Their efficiency is determined by the dimensionless figure of merit ZT: $ZT=S^2T/\rho\kappa$, where S is the Seebeck coefficient, T is the absolute temperature, ρ is the electrical resistivity, and κ is the thermal conductivity. The total thermal conductivity κ is expressed as the sum of lattice and electronic contributions ($\kappa=\kappa_l+\kappa_e$).[4,5)] κ_e can be estimated using the Wiedemann-Franz law, $\kappa_e = LT/\rho$, where L is the Lorenz number (2.44×10^{-8} $W\Omega/K^{-2}$).[5,6)] $CoSb_3$-based skutterudite compounds have attracted considerable attention as one of the best candidates of TE materials. The unfilled skutterudite $CoSb_3$ or $\square Co_4Sb_{12}$ crystallizes with the $CoAs_3$-type structure of the space group $Im\bar{3}$ (T_h^5, No. 204).[7)] The symbol □ represents a vacancy (site 2a) inside the relatively large cages, formed by the Co (site 8c) and Sb (site 24g) ions. This structure has eight formula units, including two voids □, per cubic unit cell. Although the material shows excellent thermoelectric properties (large Seebeck coefficients and high hole mobility), κ_l is very high (10 $Wm^{-1}K^{-1}$ at room temperature).[1,8)] The most interesting aspect of the skutterudite structure is that it has two large voids (site 2a) in the unit cell, which can be filled with guest ions acting as phonon rattlers.[9–11)] The 'rattling' of the filled guest ions scatters phonons and reduces κ_l. As a result, we can improve ZT by filling the voids with various guest ions such as rare-earth elements like La, Ce, and Yb and alkaline earth elements like Ba.[1,10–13)] Furthermore, double filling with guest ions such as (Ce and Yb), (In and Yb), (In and Ba), and (Ba and Yb) and multifilling such as (Ba, La, and Yb) and (Ce, In, and Yb) are also effective for improving the TE properties.[3, 11, 14–18)] This is due to the additional effects of disorder and mass fluctuation scattering of guest ions occurring between guest ions inside the voids and lattice.[19)] The reduction in κ_l for a partially filled skutterudite is one promising method for improving the TE performance. A partially filled $CoSb_3$-based skutterudite provides an increase in ZT compared with unfilled $CoSb_3$.[9,13,20)] For several partially filled skutterudite compounds, κ_l decreases with increasing filling ratio x of guest ions. Therefore, partially filled skutterudite compounds with high filling ratio are expected for high-performance TE materials. High pressure benefits the entrance of guest ions into the voids of the filled skutterudite structure than ambient pressure. Actually, it was reported that highly Yb-filled

$Yb_xCo_4Sb_{12}$ synthesized under high pressure (the actual filling ratio of Yb is 0.29) exhibits a large reduction in κ_l. The lowest κ_l of 2.02 $WK^{-1}m^{-1}$ was achieved at room temperature.[13] Furthermore, the highly mischmetal (Mm)-filled skutterudite $Mm_{0.6}Co_4Sb_{12}$, prepared by using a high-pressure technique, exhibits a low κ_l of 1.34 $WK^{-1}m^{-1}$ and shows a relatively high ZT of 0.25 at 700 K.[2] The large reduction in κ_l suggests that the rattling effect and mass fluctuation scattering are significant in this system. Mm is an alloy of rare-earth elements in various naturally occurring proportions. A typical composition includes approximately 50% Ce and 25% La, with small amounts of Nd and Pr.[21,22] If we can determine the ideal proportion of Mm (the best combination of elements) instead of the nature proportion, the TE performance could be improved for the system. To select the best combination of elements, it is important to investigate the filling effect of each element individually.

In this study, $Ce_xCo_4Sb_{12}$ and $Nd_xCo_4Sb_{12}$ were prepared by the high-pressure and high-temperature (HPHT) synthesis method. The structure and chemical composition of the samples were studied and the actual Ce and Nd filling ratios were estimated. The electrical and thermal transport properties were studied for selected compounds.

2. Experimental methods

$Ce_xCo_4Sb_{12}$ ($0 \leq x \leq 1.0$) and $Nd_xCo_4Sb_{12}$ ($0 \leq x \leq 1.0$) samples were prepared under HPHT using a Kawai-type multianvil apparatus (6-8 system). Highly pure metals of Ce (99.9%) and Nd (99.9%), Co (99.9%), and Sb (99.9999%) were used as starting materials. Ce or Nd chips, Co and Sb powders were mixed in stoichiometric ratios of $x : 4 : 12$ ($0 \leq x \leq 1.0$) and then placed in a boron nitride (BN) crucible. The BN crucible with a graphite heater surrounded with a zirconia thermal insulator was inserted into a magnesia octahedron container. The sample preparation method was described in detail in a previous paper.[10] The reaction temperature and pressure were 600 °C and 4 GPa.

The samples were characterized by X-ray diffraction (XRD) analysis (Rigaku RINT-RAPID-XG) using Co $K\alpha_1$ radiation and silicon as a standard. The chemical compositional analysis was conducted by scanning electron microscopy (SEM) with energy-dispersive X-ray spectrometry (EDX) (JEOL 6510). For the point analysis, 8 to 10 different points were carefully chosen to reduce errors.

The samples prepared under high pressure were sometimes fragile and easy to break into small pieces or powder particles, which are not suitable for evaluating the TE properties. Therefore, we combined the HPHT synthesis method using a multianvil press

and the spark plasma sintering (SPS) method. First, we removed the impurity phases of the samples prepared under high pressure and ground the samples into powder. Then, the powder was sintered by SPS at 60 MPa and 600 °C for 120 min to obtain large and dense bulk samples suitable for evaluating the properties with a high-temperature region. The samples were shaped into discoid forms with a diameter of 10 mm and a height of 2 mm. The discoid samples were used for thermal conductivity measurements with a laser flash method in vacuum using an NETZSCH LFA457 system at $T > 300$ K. The method involves the calculation of thermal conductivity from the density, thermal diffusivity, and heat capacity. For other measurements, the discoid samples were cut into rectangles with a width of 2 mm, a height of 2 mm, and a length of 8 mm. The electrical resistivity and Seebeck coefficient were measured using an ULVAC ZEM-3 system at $T > 300$ K. The thermal conductivity and Seebeck coefficient were measured using a thermal transport option of the the Physical Property Measurement System (PPMS, Quantum Design Inc.) at $T < 300$ K. The electrical resistivity was measured with the standard dc four-probe method at $T < 300$ K. Hall effect measurements were performed using the van der Pauw method under magnetic fields of 7 and -7 T by applying an electric current of 3 mA. Specific heat measurement was carried out by a thermal relaxation method (Quantum Design PPMS).

3. Results and discussion

3.1 Characterization of $Ce_xCo_4Sb_{12}$ and $Nd_xCo_4Sb_{12}$

The powder XRD patterns of $CoSb_3$ and selected samples of $Ce_xCo_4Sb_{12}$ and $Nd_xCo_4Sb_{12}$ prepared under high pressure are shown in Fig. 1. The starting materials of the selected samples are mixtures of Ce or Nd chips and Co and Sb powders in the atomic ratio of Ce or Nd : Co : Sb = 1 : 4 : 12, namely, nominal compositions are $Ce_{1.0}Co_4Sb_{12}$ and $Nd_{1.0}Co_4Sb_{12}$. Although small amounts of secondary phases of Sb and $CoSb_2$ were detected, most of the observed peaks were indexable using the skutterudite structure. The diffraction peaks of $Ce_{1.0}Co_4Sb_{12}$ and $Nd_{1.0}Co_4Sb_{12}$ shift to a low angle side, compared with those of $CoSb_3$ (inset of Fig. 1). This suggests that lattice constants increase with Ce or Nd filling. A shoulder structure of the diffraction peaks for $Nd_{1.0}Co_4Sb_{12}$ was observed at high angles. This could be due to small amounts of isostructural phases of slightly Nd-filled or unfilled Co_4Sb_{12}. Figures 2 and 3 show the lattice constants determined by a least-squares fit to the data for all $Ce_xCo_4Sb_{12}$ and $Nd_xCo_4Sb_{12}$ samples prepared under high pressure as a function of the Ce and Nd nominal filling ratio x, respectively, comparing them with the reported

data for the samples prepared at ambient pressure. The lattice constants of $Ce_xCo_4Sb_{12}$ and $Nd_xCo_4Sb_{12}$ prepared at ambient pressure increase with the Ce or Nd nominal filling ratio x and saturate above x = 0.1-0.2.[12, 23] The saturated lattice constants of the Ce and Nd filling compounds are 9.0457 Å and 9.0415 Å. The corresponding actual compositions are x = 0.1 for Ce and 0.13 for Nd, respectively. On the basis of theoretical calculations, Mei *et al*. estimated the filling fraction limit (FFL) of Ce and Nd for $\square_xCo_4Sb_{12}$ to be x = 0.1 and 0.05, respectively.[24] The experimentally obtained actual composition of $Ce_xCo_4Sb_{12}$ prepared at ambient pressure is in good agreement with the theoretical calculation. For $Nd_xCo_4Sb_{12}$, the experimental value is higher than the calculated value. On the other hand, the lattice constants of the samples prepared at 4 GPa exhibit a similar behavior and the saturated values are 9.117 Å for Ce and 9.111 Å for Nd. The actual composition, estimated by SEM and EDX by point analysis, was found to be x = 0.37 for Ce and 0.33 for the Nd-filled skutterudite, which are significantly higher than the theoretical calculations and the values of the samples prepared at ambient pressure. Therefore, the HPHT synthesis method is effective for increasing the FFL of guest ions.

To prepare large bulk samples for the evaluation of the TE properties, we employed an SPS apparatus by using the powdered samples prepared under high pressure. We could obtain large and dense bulk samples suitable for evaluating the properties. However, the actual filling ratio x of guest ions unexpectedly decreased to x = 0.13 for the Ce-filled skutterudite and 0.17 for the Nd-filled skutterudite. The lower filling ratios could be due to the lower pressure of the SPS technique. For the following sections, we express the samples as $Ce_{0.13}Co_4Sb_{12}$ and $Nd_{0.17}Co_4Sb_{12}$ by actual compositions.

3.2 Thermoelectric properties of $Ce_{0.13}Co_4Sb_{12}$ and $Nd_{0.17}Co_4Sb_{12}$

Figure 4 shows the temperature dependence of the electrical resistivity ρ for $Ce_{0.13}Co_4Sb_{12}$ and $Nd_{0.17}Co_4Sb_{12}$ prepared by HPHT synthesis and SPS techniques. The data above 300 K for $CoSb_3$ are taken from Ref. 25. Although $CoSb_3$ shows a semiconducting behavior, Ce- and Nd-filled samples exhibit a semimetallic behavior. Furthermore, the ρ values of $Ce_{0.13}Co_4Sb_{12}$ and $Nd_{0.17}Co_4Sb_{12}$ are much lower than that of $CoSb_3$. This suggests that they are heavily doped semiconductors, which can be attributed to the increase electron concentration caused by the filling of guest ions with high filling ratio.

The temperature dependence of the Seebeck coefficient S for $Ce_{0.13}Co_4Sb_{12}$ and $Nd_{0.17}Co_4Sb_{12}$ is shown in Fig. 5. The data above 300 K for $CoSb_3$ are also taken from Ref. 25. Although the S of $CoSb_3$ is positive, those of $Ce_{0.13}Co_4Sb_{12}$ and $Nd_{0.17}Co_4Sb_{12}$ are

negative, indicating transition from p-type to n-type conductors. The absolute S values reach maxima of 185 μV/K at 480 K for $Ce_{0.13}Co_4Sb_{12}$ and 166 μV/K at 690 K for $Nd_{0.17}Co_4Sb_{12}$.

Figures 6 and 7 show the temperature dependences of the carrier concentration n and carrier mobility μ for $Ce_{0.13}Co_4Sb_{12}$ and $Nd_{0.17}Co_4Sb_{12}$, respectively. n and μ were calculated from the Hall coefficient R_H, namely, $n = 1/(eR_H)$ and $\mu = R_H/\rho$, where e is the elementary charge. The observation of negative Hall coefficients for both $Ce_{0.13}Co_4Sb_{12}$ and $Nd_{0.17}Co_4Sb_{12}$ is consistent with the Seebeck coefficients. The n values of both $Ce_{0.13}Co_4Sb_{12}$ and $Nd_{0.17}Co_4Sb_{12}$ increase with temperature because of the increased activation of charge carriers across the band gap, while that of $CoSb_3$ is nearly constant in the temperature range of 150–300 K. By filling Ce or Nd, n increases to 2.6×10^{20} cm^{-3} and 7.6×10^{20} cm^{-3} for $Ce_{0.13}Co_4Sb_{12}$ and $Nd_{0.17}Co_4Sb_{12}$, respectively, from 0.036×10^{20} cm^{-3} ($CoSb_3$) at 300 K. The μ values of both $Ce_{0.13}Co_4Sb_{12}$ and $Nd_{0.17}Co_4Sb_{12}$ decrease with increasing temperature, while that of $CoSb_3$ increases (Fig. 7). The μ values at room temperature decrease to 7.86 and 8.66 $cm^2V^{-1}s^{-1}$ for $Ce_{0.13}Co_4Sb_{12}$ and $Nd_{0.17}Co_4Sb_{12}$, respectively from 220.99 $cm^2V^{-1}s^{-1}$ for $CoSb_3$. The μ values of both compounds exhibit a $T^{-3/2}$ behavior above 150 K. The results suggest that the carrier scattering mechanism is mainly acoustic phonon scattering.

Figure 8 shows the temperature dependences of the total thermal conductivity κ [Fig. 8(a)] and lattice thermal conductivity κ_l [Fig. 8(b)] in the temperature range from 5 to 760 K for $Ce_{0.13}Co_4Sb_{12}$ and $Nd_{0.17}Co_4Sb_{12}$. The data above 300 K for $CoSb_3$ are taken from Ref. 25. By filling Ce or Nd, both κ and κ_l decrease. The minimum κ_l values are 2.57 $Wm^{-1}K^{-1}$ at 670 K and 2.11 $Wm^{-1}K^{-1}$ at 680 K for $Ce_{0.13}Co_4Sb_{12}$ and $Nd_{0.17}Co_4Sb_{12}$, respectively. A reduction in κ_l suggests the rattling of Ce or Nd atoms. Furthermore, the random distribution of partly filled Ce or Nd ions in vacant sites causes a more effective phonon scattering. The difference in the reduction of κ_l between Ce and Nd ions, having almost the same content as filling guest ions, could be due to the differences in the mass and size of guest ions. The small and heavy rattler tends to induce a more off-center behavior than the large and light ions. Therefore, the κ_l of the Nd-filled skutterudite is lower than that of the Ce-filled skutterudite because Nd has a smaller ionic radius and a larger mass than Ce.

The low-temperature specific heat C was measured for $Ce_{0.13}Co_4Sb_{12}$ and $Nd_{0.17}Co_4Sb_{12}$ to investigate the contribution of localized incoherent motions of guest ions in the vacancy site of the skutterudite structure. The low-temperature specific heat C can

be fitted by $C(T) = \gamma T+\beta T^3$ (Debye T^3 law), where γ is the electronic specific heat coefficient and the Debye temperature $\Theta_D = (12\pi^4 R_g n/5\beta)^{1/3}$ (R_g is the gas constant and n is the number of atoms/f.u.). Thus, γ and Θ_D are estimated (Table I). To investigate the Einstein vibration at low temperatures, the specific heat C was plotted in $(C - \gamma T)/T^3$ vs temperature as shown in Fig. 9. The temperature dependence of $(C - \gamma T)/T^3$ for $CoSb_3$ deviates from the simple Debye behavior, although $CoSb_3$ has no filler guest ions. This could be attributed to the low-energy optical phonons of the Sb_4 ring.[26, 27] $Ce_{0.13}Co_4Sb_{12}$ and $Nd_{0.17}Co_4Sb_{12}$ exhibit an enhanced large broad maximum at around 20 K, which should be attributed to the Ce or Nd filler ions. The Einstein temperature Θ_E can be estimated with the relation $\Theta_E = 4.92\ T_{max}$, where T_{max} is the maximum temperature in $(C - \gamma T)/T^3$. Note that the T_{max} (namely, Θ_E) values of $Ce_{0.13}Co_4Sb_{12}$ and $Nd_{0.17}Co_4Sb_{12}$ become lower than that of $CoSb_3$. The estimated Θ_E values are also listed in Table I. The reduction in Θ_E suggests that low-energy optical modes (LGOMs) shifted to lower temperatures.

Figure 10 shows the temperature dependence of the dimensionless figure of merit (ZT). The maximum ZT values of 0.26 and 0.48 were achieved at 700 K for $Ce_{0.13}Co_4Sb_{12}$ and $Nd_{0.17}Co_4Sb_{12}$, respectively. These values are higher than the ZT of 0.25 at 700 K for the mischmetal (Mm)-filled skutterudite $Mm_{0.6}Co_4Sb_{12}$ prepared by the HTHP method.[2] The increase in ZT is mainly due to the filling of guest ions and the change in carrier concentration. The use of HPHT synthesis can not only make it possible to fill a wide variety of elements into Sb vacancies, but also increase the upper limit of elements. The high filling ratio of Ce or Nd ions in voids of $CoSb_3$ results in the improvement of the thermoelectric performance. Unfortunately, the use of the SPS technique causes a deviation from the expected compositions, namely, a reduction in the filling ratio of guest ions. We should develop a new technique of fabricationg large bulk samples while keeping a high filling rate of samples prepared by HPHT synthesis.

4. Conclusions

In this study, we have successfully synthesized n-type filled skutterudites by the HPHT technique. The actual Ce and Nd filling rates indicate an advantage of the HPHT technique, which can substantially increase the filling fraction into the voids of $CoSb_3$, compared with conventional synthesis techniques. The high filling fraction rate results in a significant suppression of κ_l. The lowest κ_l of this study is 2.11 W/mK at 680 K for $Nd_{0.17}Co_4Sb_{12}$. The maximum ZT values of $Ce_{0.13}Co_4Sb_{12}$ and $Nd_{0.17}Co_4Sb_{12}$ are 0.26 and 0.48 at 700 K, respectively. This work suggests that Nd filling is much effective for the improvement of

the TE performance of $CoSb_3$-based compounds. Furthermore, the κ_l of double-filled or multifilled skutterudite compounds is generally lower than that of single-filled compounds, which indicates the possibility of inducing a lower κ_l by synthesizing double-filled or multifilled skutterudites prepared by HPHT synthesis. Mm includes various rare-earth elements (50% Ce and 25% La, with small amounts of Nd and Pr). Therefore, if we use Nd-rich Mm, namely, "artificial Mm" instead of the natural Mm, the TE performance could be improved. In this manner, the HPHT technique is one of the most attractive approaches to fabricating n-type filled skutterudite compounds, with the advantages of increasing filling fraction and marked reduction in lattice thermal conductivity.

Acknowledgments

This work was partially supported by a Grant-in-Aid for Scientific Research (Nos. 23340092, 15K17687, and 16K06810) from the Japan Society for the Promotion of Science. This work was also partially supported by CREST (No. JPMJCR16Q6) from the Japan Science and Technology Agency and by the New Energy and Industrial Technology Development Organization through the Thermal Management Materials and Technology Research Association.

References

1) G. S. Nolas and G. Fowler, J. Mater. Res. **20**, 3234 (2005).

2) C. Sekine, H. Kato, Y. Kawamura, and C.-H. Lee, Mater. Sci. Forum **879**, 1737 (2017).

3) X. Shi, J. Yang, J. R. Salvador, M. F. Chi, J. Y. Cho, H. Wang, S. Q. Bai, J. H. Yang, W. Q. Zhang, and L. D. Chen, J. Am. Chem. Soc. **133**, 7837 (2011).

4) B. Bourgoin, D. Bérardan, E. Alleno, C. Godart, O. Rouleau, and E. Leroy, J. Alloys. Compd. **399**, 47 (2005).

5) D. M. Rowe, *CRC Handbook of Thermoelectrics* (CRC Press, Boca Raton, FL, 1995) Chap. 20.

6) G. S. Nolas, D. T. Morelli, and T. M. Tritt, Annu. Rev. Mater. Sci. **29**, 89 (1999).

7) N. Mandel and J. Donohue, Acta Crystallogr., Sect. B **27**, 2288 (1971).

8) D. T. Morelli, T. Caillat, J.-P. Fleurial, A. Borshchevsky, J. Vandersande, B. Chen, and C. Uher, Phys. Rev. B **51**, 9622 (1995).

9) X. F. Tang, L. D. Chen, T. Goto, and T. Hirai, J. Mater. Res. **16**, 837 (2001).

10) C. Sekine and Y. Mori, Jpn. J. Appl. Phys. **56**, 05FA09 (2017).

11) X. Shi, H. Kong, C. P. Li, C. Uher, J. Yang, J. R. Salvador, H. Wang, L. Chen, and W.

Zhang, Appl. Phys. Lett. **92**, 182101 (2008).

12) D. T. Morelli, G. P. Meisner, B. Chen, S. Hu, and C. Uher, Phys. Rev. B **56**, 7376 (1997).

13) Y. Chen, Y. Kawamura, J. Hayashi, and C. Sekine, Jpn. J. Appl. Phys. **54**, 055501 (2015).

14) X. Shi, S. Bai, L. Xi, J. Yang, W. Zhang, L. Chen, and J. Yang, J. Mater. Res. **26**, 1745 (2011).

15) J. Graff, J. He, and T. M. Tritt, Inorganics **2**, 168 (2014).

16) D. Hobbis, Y. Liu, K. Wei, T. Tritt, and G. Nolas, Crystals **7**, 256 (2017).

17) L. Deng, J. Ni, L. B. Wang, X. P. Jia, J. M. Qin, and B. W. Liu, J. Alloys Compd. **712**, 477 (2017).

18) L. Deng, L. B. Wang, J. Ni, J. M. Qin, X. P. Jia, and H. A. Ma, Mater. Lett. **217**, 44 (2018).

19) G. P. Meisner, D. T. Morelli, S. Hu, J. Yang, and C. Uher, Phys. Rev. Lett. **80**, 3551 (1998).

20) L. Wang, K. F. Cai, Y. Y. Wang, H. Li, and H. F. Wang, Appl. Phys. A **97**, 841 (2009).

21) L. Zhang, A. Grytsiv, M. Kerber, P. Rogl, E. Bauer, and M. Zehetbauer, J. Alloys. Compd. **490**, 19 (2010).

22) C. Sekine, H. Kato, M. Kanazawa, Y. Kawamura, K. Takeda, M. Matsuda, K. Kihou, C.-H. Lee, and H. Gotou, J. Phys. Conf. Ser. **502**, 012017 (2014).

23) V. L. Kuznetsov, L. A. Kuznetsova, and D. M. Rowe, J. Phys. Condens. Matter **15**, 5035 (2003).

24) Z. G. Mei, W. Zhang, L. D. Chen, and J. Yang, Phys. Rev. B **74**, 153202 (2006).

25) K.-H. Park and W.-S. Seo, J. Korean Phys. Soc. **65**, 491 (2014).

26) V. Keppens, D. Mandrus, B. Sales, B. Chakoumakos, P. Dai, R. Coldea, M. Maple, D. Gajewski, E. Freeman, and S. Bennington, Nature **395**, 876 (1998).

27) I. K. Dimitrov, M. E. Manley, S. M. Shapiro, J. Yang, W. Zhang, L. Chen, Q. Jie, G. Ehlers, A. Podlesnyak, and J. Camacho, Phys. Rev. B **82**, 174301 (2010).

Figure Captions

Fig. 1. (Color online) XRD patterns of nominal-composition $Ce_{1.0}Co_4Sb_{12}$, $Nd_{1.0}Co_4Sb_{12}$ and Co_4Sb_{12} synthesized at 4 GPa. Secondary phases of Sb and $CoSb_2$ are indicated by solid circles and stars, respectively.

Fig. 2. (Color online) Lattice constants of nominal-composition $Ce_xCo_4Sb_{12}$ synthesized at high pressure (4 GPa) along with the reported values of $Ce_xCo_4Sb_{12}$ synthesized at ambient pressure.[12)]

Fig. 3. (Color online) Lattice constants of nominal-composition $Nd_xCo_4Sb_{12}$ synthesized at high pressure (4 GPa) along with the reported values of $Nd_xCo_4Sb_{12}$ synthesized at ambient pressure.[23)]

Fig. 4. (Color online) Temperature dependence of the electrical resistivity ρ for $Ce_{0.13}Co_4Sb_{12}$ and $Nd_{0.17}Co_4Sb_{12}$. The data above 300 K for $CoSb_3$ are taken from Ref. 25.

Fig. 5. (Color online) Temperature dependence of the Seebeck coefficient S for $Ce_{0.13}Co_4Sb_{12}$ and $Nd_{0.17}Co_4Sb_{12}$. The data above 300 K for $CoSb_3$ are taken from Ref. 25.

Fig. 6. (Color online) Temperature dependence of carrier concentration n for $Ce_{0.13}Co_4Sb_{12}$ and $Nd_{0.17}Co_4Sb_{12}$.

Fig. 7. (Color online) Temperature dependence of carrier mobility μ for $Ce_{0.13}Co_4Sb_{12}$ and $Nd_{0.17}Co_4Sb_{12}$.

Fig. 8. (Color online) Temperature dependences of the total thermal conductivity κ (a) and lattice thermal conductivity κ_l (b) for $Ce_{0.13}Co_4Sb_{12}$ and $Nd_{0.17}Co_4Sb_{12}$. The data above 300 K for $CoSb_3$ are taken from Ref. 25.

Fig. 9. (Color Online) Temperature dependence of $(C - \gamma T)/T^3$ for $Ce_{0.13}Co_4Sb_{12}$ and $Nd_{0.17}Co_4Sb_{12}$.

Fig. 10. (Color online) Temperature dependence of figure of merit *ZT* for $Ce_{0.13}Co_4Sb_{12}$ and $Nd_{0.17}Co_4Sb_{12}$. The data for $Mm_{0.6}Co_4Sb_{12}$ and the data above 300 K for $CoSb_3$ are taken from Refs. 2 and 25, respectively.

Table I. Eelectronic specific heat coefficient γ, Θ_D, and Θ_E values of $CoSb_3$, $Ce_{0.13}Co_4Sb_{12}$, and $Nd_{0.17}Co_4Sb_{12}$.

Sample	γ (J/molK^2)	Θ_D	Θ_E
$CoSb_3$	0.0577	295.7	107
$Ce_{0.13}Co_4Sb_{12}$	0.0034	250.4	96
$Nd_{0.17}Co_4Sb_{12}$	0.0804	239.5	86

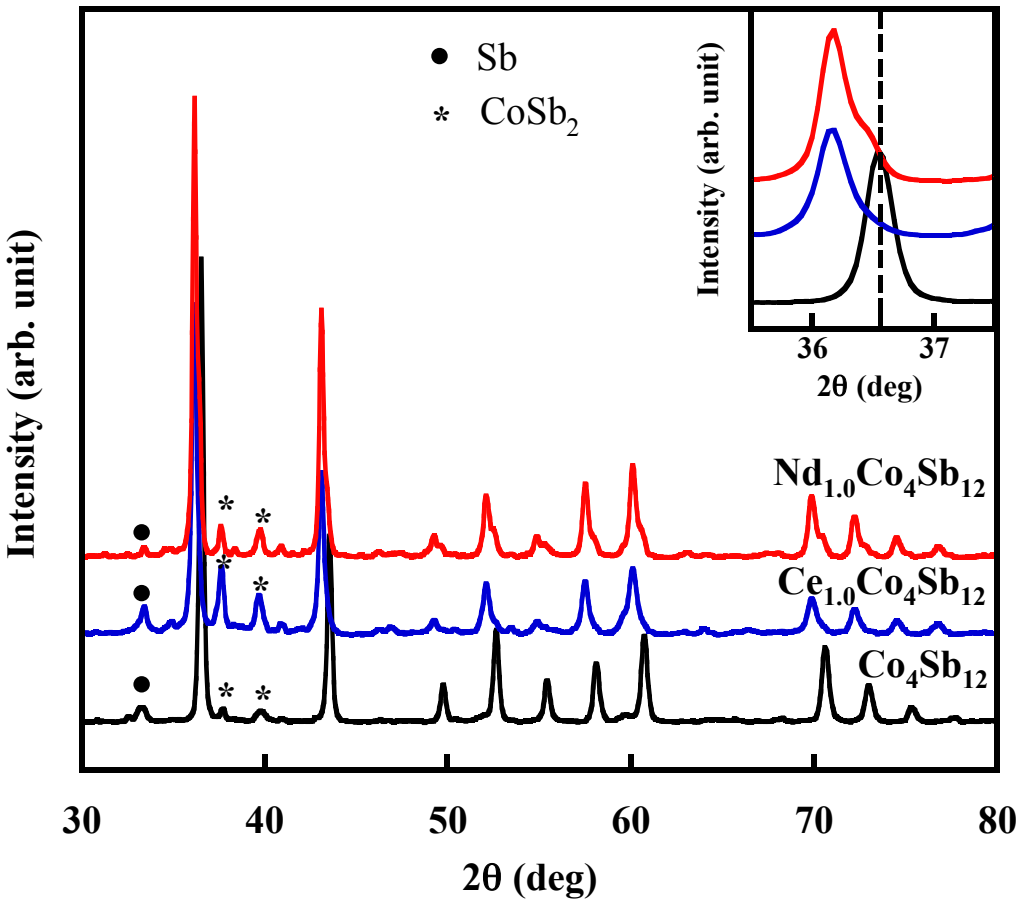

Fig. 1. (Color Online) XRD pattern of nominal-composition $Ce_{1.0}Co_4Sb_{12}$, $Nd_{1.0}Co_4Sb_{12}$ and Co_4Sb_{12} synthesized at 4 GPa. Secondary phases of Sb and $CoSb_2$ are indicated by solid circles and stars, respectively. The inset shows an enlarged figure around main peak (310).

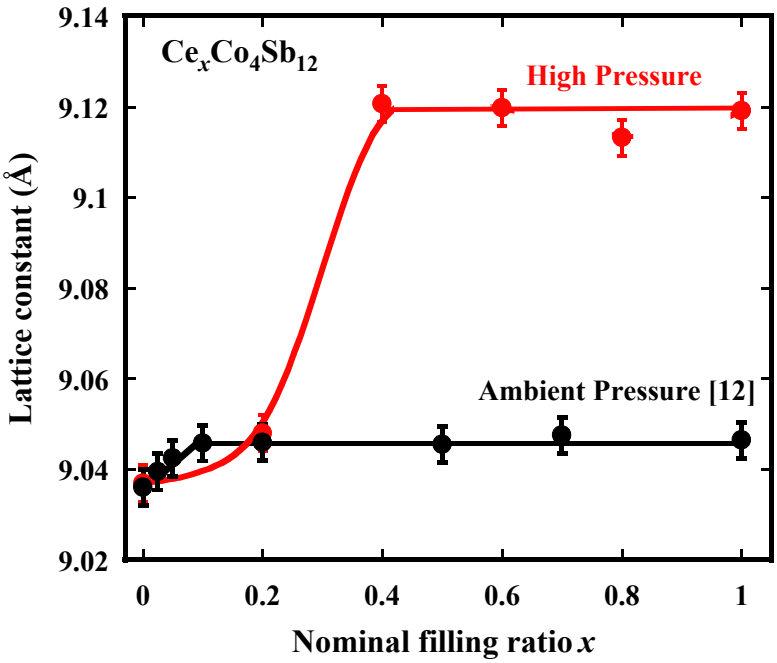

Fig. 2. (Color Online) Lattice constants of nominal-composition $Ce_xCo_4Sb_{12}$ synthesized at high pressure (4 GPa) along with the reported values of $Ce_xCo_4Sb_{12}$ synthesized at ambient pressure.[12)]

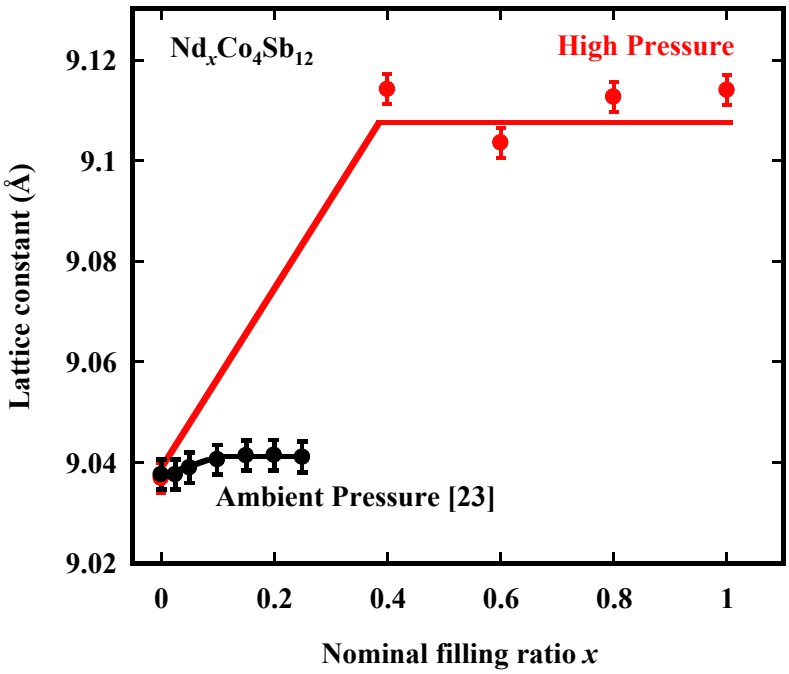

Fig. 3. (Color Online) Lattice constants of nominal-composition $Nd_xCo_4Sb_{12}$ synthesized at high pressure (4 GPa) along with the reported values of $Nd_xCo_4Sb_{12}$ synthesized at ambient pressure.[23)]

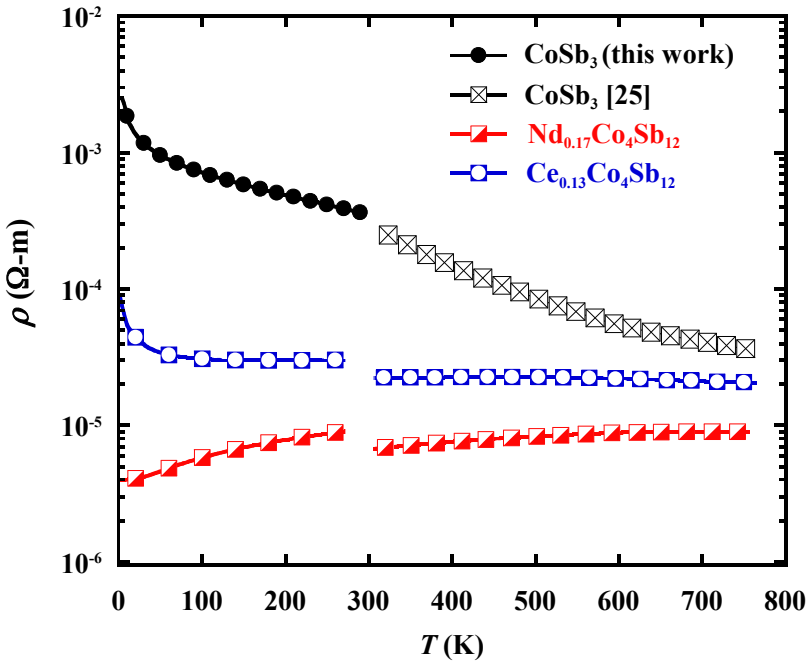

Fig. 4. (Color Online) Temperature dependence of the electrical resistivity ρ for $Ce_{0.13}Co_4Sb_{12}$ and $Nd_{0.17}Co_4Sb_{12}$. The data above 300 K for $CoSb_3$ are taken from Ref. 25.

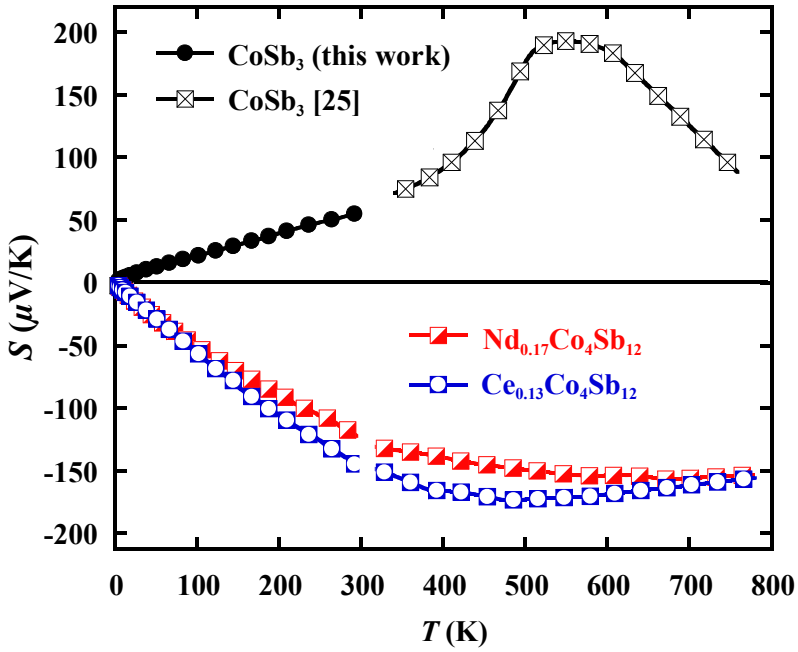

Fig. 5. (Color Online) Temperature dependence of the Seebeck coefficient S for $Ce_{0.13}Co_4Sb_{12}$ and $Nd_{0.17}Co_4Sb_{12}$. The data above 300 K for $CoSb_3$ are taken from Ref. 25.

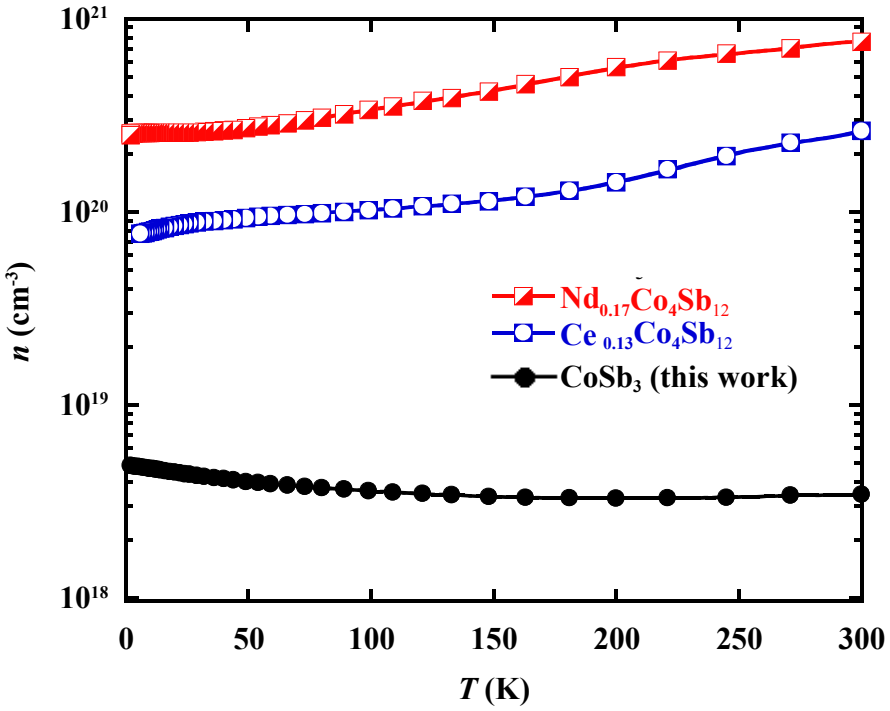

Fig. 6. (Color Online) Temperature dependence of carrier concentration n for $Ce_{0.13}Co_4Sb_{12}$ and $Nd_{0.17}Co_4Sb_{12}$.

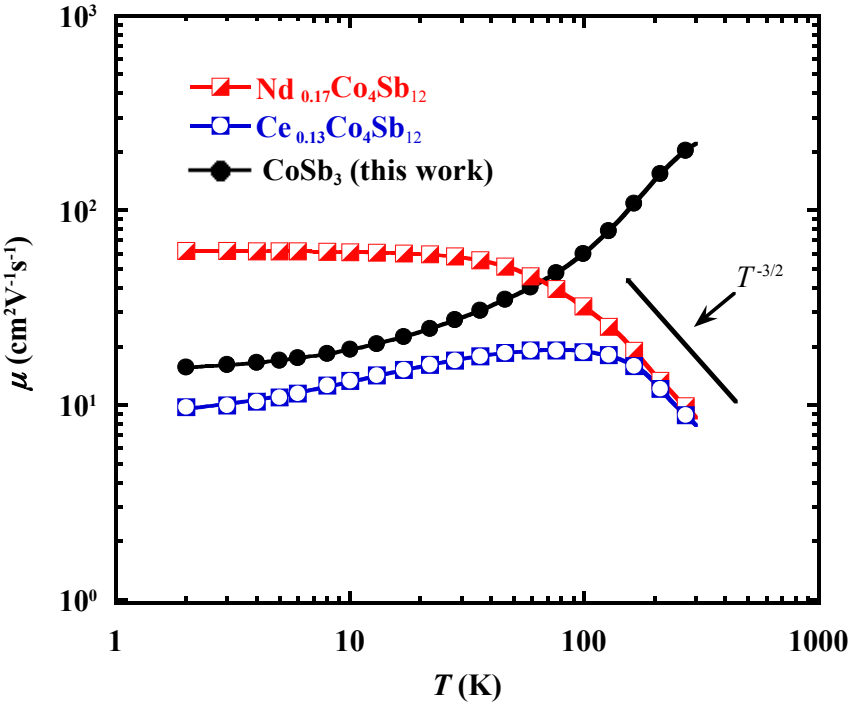

Fig. 7. (Color Online) Temperature dependence of carrier mobility μ for $Ce_{0.13}Co_4Sb_{12}$ and $Nd_{0.17}Co_4Sb_{12}$.

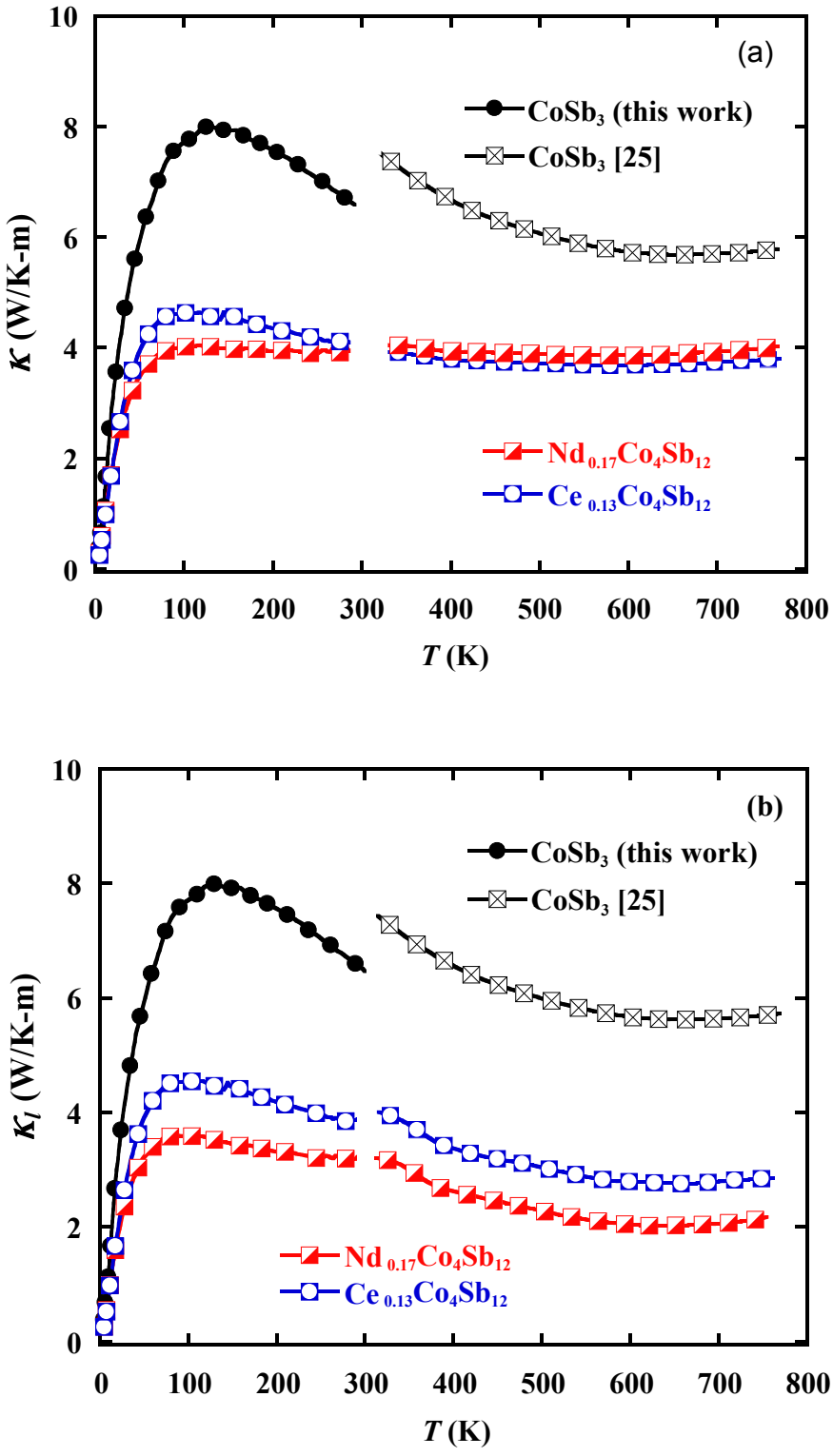

Fig. 8. (Color Online) Temperature dependences of the total thermal conductivity κ (a) and lattice thermal conductivity κ_l (b) for $Ce_{0.13}Co_4Sb_{12}$ and $Nd_{0.17}Co_4Sb_{12}$. The data above 300 K for $CoSb_3$ are taken from Ref. 25.

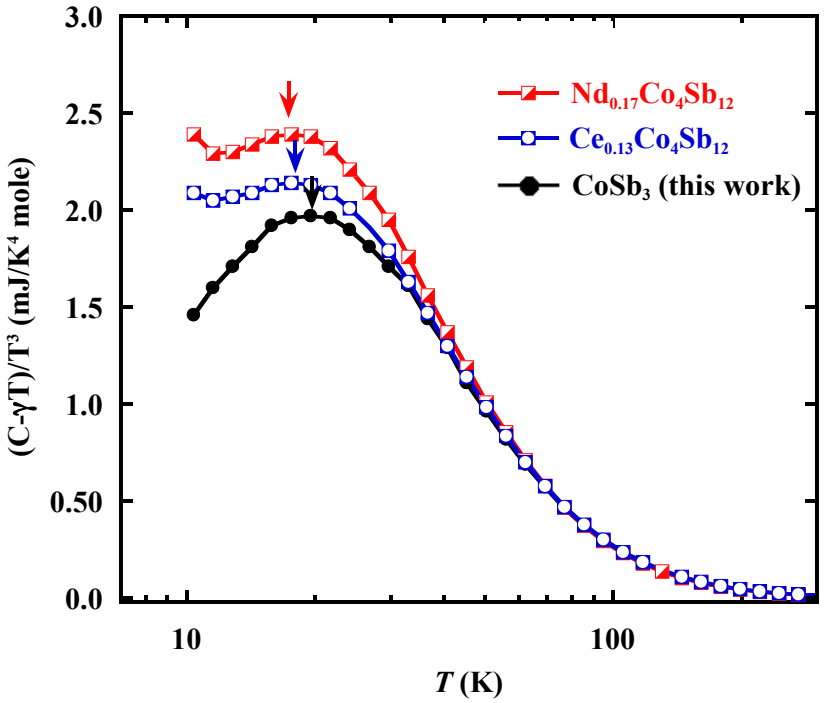

Fig. 9. (Color Online) Temperature dependence of $(C - \gamma T)/T^3$ for $Ce_{0.13}Co_4Sb_{12}$ and $Nd_{0.17}Co_4Sb_{12}$.

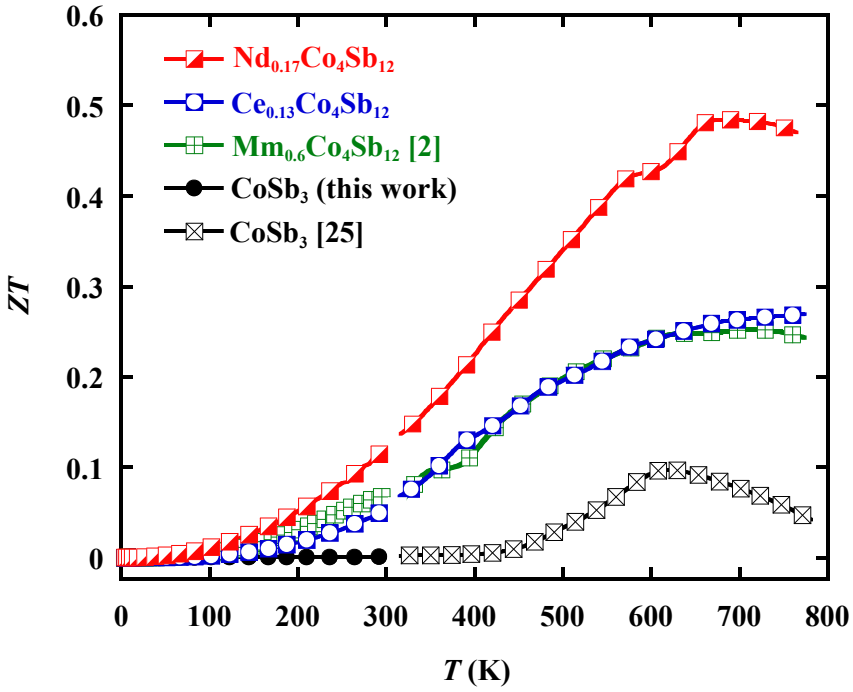

Fig. 10. (Color Online) Temperature dependence of figure of merit ZT for $Ce_{0.13}Co_4Sb_{12}$ and $Nd_{0.17}Co_4Sb_{12}$. The data for $Mm_{0.6}Co_4Sb_{12}$ and the data above 300 K for $CoSb_3$ are taken from Refs. 2 and 25, respectively.